J Comput Electron (2010) 9: 135–140
DOI 10.1007/s10825-010-0323-x

An advanced description of oxide traps in MOS transistors and its relation to DFT

F. Schanovsky · W. Gös · T. Grasser

Published online: 23 October 2010

Abstract Recently, an advanced model for defects in the insulating regions of semiconductor devices has been suggested, which can explain the removable component of the negative bias temperature instability (NBTI) and recoverable random telegraph/flicker noise. We give a brief introduction to the atomic scale physics behind the model and show how model parameters can be extracted from density functional theory (DFT) calculations. The central link between DFT calculations and device simulation is the carrier energy dependent part of the capture cross section, the line shape function. Calculations of the line shape functions of model defect structures using a simple harmonic approximation are presented. The calculations show a considerable shift in the oscillator frequency upon charge state transitions for the defects investigated.

Keywords Oxide defects · DFT · NBTI · RTS · Line shape function

1 Introduction

Point defects in solids have been in the focus of scientific interest due to their large influence on the macroscopic mechanical, electrical, and optical properties of the host material, starting from the very beginnings of solid state theory. In semiconductor device modeling, defects are primarily considered as recombination centers and described using the Shockley-Read-Hall (SRH) theory [1], which characterizes a defect via the capture cross section σ and the trap level E_{T}.

Within insulating layers, such as depletion regions or dielectrics, the major influence of defect sites on the charge carrier gas in adjacent conducting regions is through electrostatic interaction rather than recombination. Capacitive methods, such as deep-level transient spectroscopy (DLTS) [2, 3], as well as random telegraph signals (RTS) in the drain current of appropriately biased small-scale MOS transistors [4] have been used to study in detail the charging and discharging dynamics of defect centers in insulating layers, revealing a very complex behavior that requires modeling to go beyond the SRH description [4–6].

Recently, it has been proposed that the recoverable component of the negative bias temperature instability (NBTI) in MOSFETs is caused by trapping of carriers at point defects within the gate oxide [7]. The very same defects were indicated to also cause flicker ($1/f$) noise [8–10], which is (at least partly) attributed to a superposition of a multitude of RTS signatures in large-area devices. A study of the response of small scale devices to NBT stress led to the development of the time dependent defect spectroscopy (TDDS), which made a detailed investigation of the charging and discharging of single defects possible [11]. The results of these and other experiments stimulated the development of an advanced defect model applicable to the case of NBT degradation as well as RTS and $1/f$ noise.

2 Defect model

2.1 A detailed view of oxide defects

To understand the complex behavior of trapping centers it is necessary to consider the thermal motion of their atoms.

F. Schanovsky (✉) · W. Gös · T. Grasser
Gußhausstraße 27-29/E360, 1040 Vienna, Austria
e-mail: schanovsky@iue.tuwien.ac.at

W. Gös
e-mail: goes@iue.tuwien.ac.at

T. Grasser
e-mail: grasser@iue.tuwien.ac.at

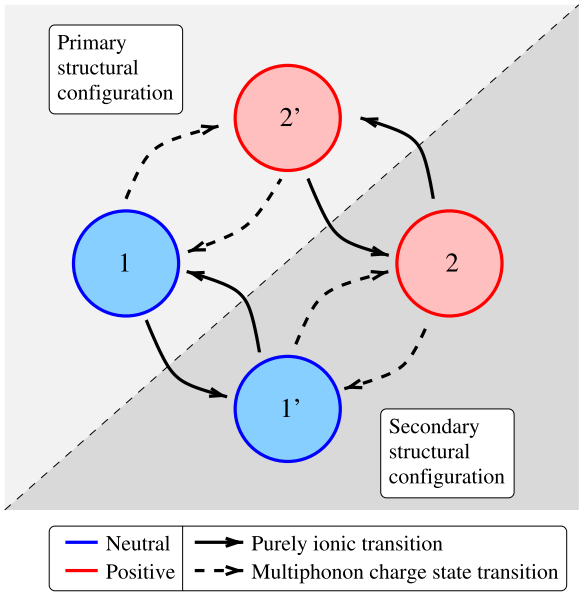

Fig. 1 States of the defect in our model for NBTI. The defect can exist in two different structural states, where each again can be either neutral or positively charged

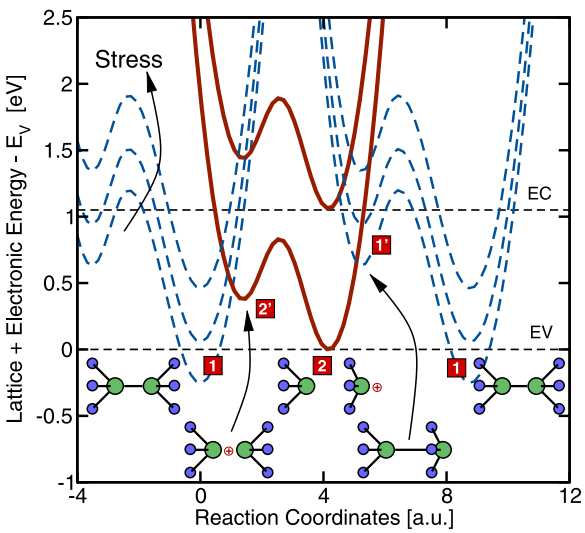

Fig. 2 The metastable states in the model are the minima of the total energy surfaces of the defect structure in its neutral (*dashed lines*) and positive (*solid lines*) states. The effects of stress and different reservoir energies are indicated [11]

These random vibrations influence the trapping dynamics [3] and give rise to chemical reactions, e.g. structural reorganization or particle exchange with other defects, at the defect site [7, 11, 12]. In our model, the different electrical and structural configurations of the defect are treated as (meta-)stable states, as shown in Fig. 1. The description of the interplay of electronic and vibrational degrees of freedom comes in the form of potential energy surfaces (see Fig. 2) which are a direct consequence of the Born-Oppenheimer approximation. The potential energy surface $E_\alpha(q)$ corresponding to a certain electronic state α assigns a total energy (i.e. the energy including all ionic and electronic interactions) to each atomic configuration q. The configuration q consists of all the positions of atoms associated with the defect. In our model, the defect is assumed to have two relevant potential energy surfaces, corresponding to the neutral and the positive state of the defect. Figure 2 shows the gradual change of the total energies as the system moves in configuration space and the resulting energetic minima which give rise to the metastable states of the defect (denoted 1, 1′, 2, and 2′). The coordinate q follows the path of minimum energy between two minima in configuration space and is sometimes called *reaction coordinate*. The transition between the metastable states occurs by thermal excitation over the separating barriers. The barriers for transitions between the charge states are defined by the crossing of the potential energy surfaces in the classical limit.

The electrons in the gate and the semiconductor bulk are considered as a reservoir with E_{res}. The total energy involving the defect and the rest of the device becomes

$$E_{\text{tot}}^{+/0} = E_{+/0}(q) + E_{\text{res}}, \quad E_{\text{res}} = \sum_i n_i E_i, \tag{1}$$

where i runs over all reservoir states, and n_i and E_i are the occupation of reservoir state i and its energy, respectively. For a neutral-to-positive transition, where an electron from the defect is moved to the nth reservoir state, the occupation in the reservoir state E_n is raised by one, so the difference between the energy in the neutral and the positive state becomes

$$E_{\text{tot},+} - E_{\text{tot},0} = E_+ - E_0 + E_n. \tag{2}$$

The consequence of (2) is that the relative position of the total energy surfaces becomes dependent on the reservoir state involved in the transition between them. Each additional reservoir state provides an additional option for the system to change the charge state of the defect, as indicated in Fig. 2 by the two solid lines representing the silicon conduction and valence level, respectively. In a real device, there will be a more or less broad spectrum of reservoir states.

2.2 Bias dependence

The effect of gate bias on the trapping process in the limit of a nearly uncharged oxide can be estimated by a simple model [13]. When the defect is approximated as an object of zero spatial extension and the reservoir states are approximated as localized at the oxide/semiconductor or oxide/metal interface, an electric field F in the oxide induces an additional potential difference that an electron experiences when traveling between the defect and the reservoir.

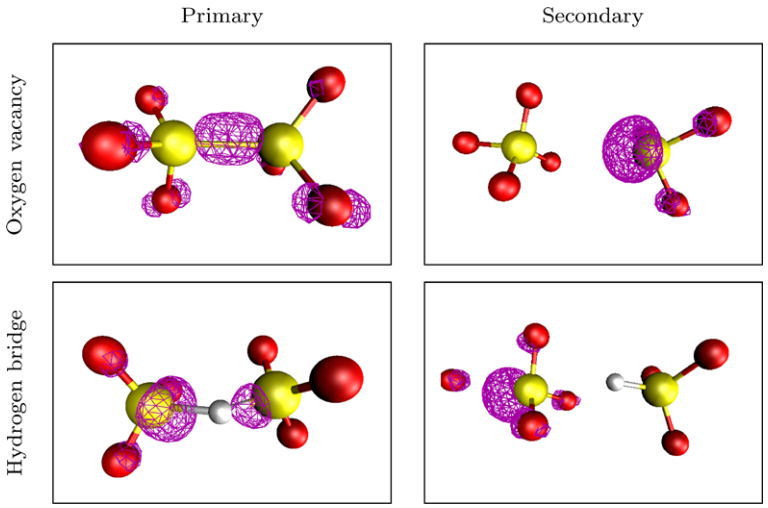

Fig. 3 Optimized defect structures for the oxygen vacancy and the hydrogen bridge in the primary as well as the secondary state (all neutral). The electron density of the localized Kohn-Sham-eigenstate is shown as wireframe. Our structural parameters are in excellent agreement with those of [12]

The magnitude of this potential difference is $e_0 x F$, where e_0 is the elementary charge and x is the effective distance between the defect and the interface. This adds to the difference between the neutral and positively charged defect state, as indicated in Fig. 2 by the dashed lines. This estimation is of course only qualitative. When considering real devices, the reservoir energies with respect to the defect have to be taken from a self-consistent calculation.

2.3 Degradation and recovery

In our model, the defect is initially in state 1, which is electrically neutral. During normal device operation, the defect will remain there due to the large energetic barriers separating state 1 from all other states. When large negative bias is applied, the relative shift of the neutral potential energy surface to the positive ones changes as indicated in Fig. 2, resulting in a decrease of the transition barrier for hole capture from the silicon valence band. After the transition to the positive state ($1 \rightarrow 2'$), the defect undergoes structural relaxation and moves to state 2 by overcoming a small energetic barrier. In its new (secondary) structural configuration, even after the bias is removed, the defect can change its charge state much easier, due to the smaller barriers for interaction with the silicon. From the neutral secondary state $1'$, the defect can return to the initial configuration by again overcoming a thermal barrier.

In electrical measurements one observes a large ensemble of the described defects and, due to the amorphous nature of the gate oxide, every defect moves on a different energetic landscape. This means that all the state energies and barrier energies are statistically distributed and thus each defect shows a different transient behavior. The superposition of a large number of defects changing their state from 1 to 2, e.g. due to electrical stress, is observed as a degradation of the device characteristics, as the charge carriers in the silicon substrate are influenced by the electric field of the defects. Similarly, if an increased number of defects undergo the transition $1' \rightarrow 1$, a recovery of device characteristics will be observed macroscopically.

3 Charge transitions from DFT

The potential energy surfaces can be directly calculated from DFT for a given bulk defect structure. In those calculations the number of electrons in the system can be manually adjusted, which makes the computation of different charge states possible. To build on a sound foundation, we selected well studied defect structures for our calculations: the oxygen vacancy and the hydrogen bridge. As shown in Fig. 3, both defects have a primary as well as a secondary configuration. The oxygen vacancy has been proposed to be relevant for several observed effects, such as radiation damage [14] or flicker noise [15]. The hydrogen bridge has been proposed as the defect causing stress-induced leakage current (SILC) [12, 16]. We use alpha quartz as a host structure, since it is a well-studied reference for amorphous silica [12, 17, 18]. We calculated the properties of the defect models, focussing on the charge state transitions $1 \leftrightarrow 2'$ and $2 \leftrightarrow 1'$ (see Fig. 1). The calculations were performed using the Vienna ab initio simulation program (VASP) [19, 20]. The host structure supercell contains 72 atoms, the wave functions are expanded in a plane-wave basis set up to 800 eV. The k-space is sampled at the Γ-point. The core electrons are treated using the projector augmented wave (PAW) method, the PAW parameters are taken from the VASP PAW database.

In our model, charge transitions are treated using non-radiative multi phonon (NMP) transition theory, which has been used by several authors for the description of defects in semiconductors [3, 5, 13]. In NMP transitions the non-

radiative capture cross section from an initial electronic state i to a final state f is expressed as

$$\sigma_{\mathrm{if}} = A_{\mathrm{if}}\, f, \tag{3}$$

where A_{if} depends only on the electronic degrees of freedom, and f describes the vibrational influence.

A_{if} contains the electronic matrix element of the initial and the final state [3, 7, 21]. This matrix element includes the electronic wave functions of the reservoir states, thus it cannot be obtained from an atomistic bulk defect calculation. Instead, this quantity has to be estimated during a device simulation [5, 7, 22]. Useful estimates can be taken from classical (e.g. drift-diffusion) device simulations by approximating the electronic matrix element with a tunnelling term (e.g. WKB).

The line shape function f in its most general form is based on overlaps of the different vibrational wave functions corresponding to the initial and the final electronic state [23]. It reads

$$f = \operatorname*{avg}_{\eta_{\mathrm{i}}} \sum_{\eta_{\mathrm{f}}} \left|\langle \eta_{\mathrm{f}} | \eta_{\mathrm{i}} \rangle\right|^2 \delta(E_{\eta_{\mathrm{f}}} - E_{\eta_{\mathrm{i}}}). \tag{4}$$

η_{i} denotes the initial vibrational wave functions and η_{f} the final ones. The transition probability from a certain η_{i} to a η_{f} is determined by the overlap of the two vibrational wave functions times the Dirac peak, which represents the conservation of energy. Prior to the transition, the system will be in thermal equilibrium, so the probability of finding the system in a certain vibrational state η_{i} is determined by thermal statistics, expressed by the thermal average over the initial states.

The vibrational wave functions and their associated energies are determined by the potential energy surfaces of the initial and final state of the electronic system, which are the neutral and the positively charged defect in our case. The energies, and in consequence the line shape function, follow the dependence of the potential energy surfaces on the reservoir and the bias. In consequence, the line shape function can be interpreted as the carrier-energy dependent part of the capture cross section for transitions sharing the same electronic matrix element.

In principle, as long as non-adiabatic effects do not play a role, one would have to take the 3N-dimensional (where N is the number of atoms) potential energy surface from DFT and solve the Schrödinger equation for the nuclei. As this is not feasible, it is necessary to reduce the complexity of the problem by making approximations. We have proposed a simple method to extract approximated vibrational wave functions from DFT calculations [21], relying on the assumptions of single mode coupling and parabolic potential energy surfaces. This method was applied to the study of defect models in relation to our model for NBTI. The expressions for the neutral and positive defect read

$$E_0(q) = \frac{M\omega_0^2}{2} q^2, \qquad E_+(q) = \frac{M\omega_+^2}{2}(q - q_{\mathrm{s}})^2 + E_{\mathrm{s}}. \tag{5}$$

The parameters M, ω_0, ω_+, E_{s}, and q_{s} are extracted from DFT calculations in the neutral and positive state at the neutral and positive optimum configurations, as indicated in Fig. 4. As the potential energies for both electronic states are assumed to be parabolic, the corresponding vibrational wave functions are harmonic oscillator wave functions. The overlap integral becomes

$$\langle \eta_{\mathrm{f}} | \eta_{\mathrm{i}} \rangle = \langle \omega_+, m | \omega_0, n \rangle, \tag{6}$$

where $|\omega, i\rangle$ is the i-th eigenvector of the harmonic oscillator of frequency ω. Several analytic expressions for this integral can be found in literature, e.g. [24] and [25]. Numerical evaluation of these expressions, however, becomes problematic for high quantum numbers (>100) using finite precision floating point arithmetics, therefore we calculated the overlap integrals using numerical integration of the products of the analytic expressions for the harmonic oscillator wave functions.

4 Results

The employed defect structures are shown in Fig. 3. The structures were relaxed until the forces were below 10^{-2} eV/Å. We compared the structural parameters with [12] and found excellent agreement for all states.

Figure 4 shows the extracted potential energy surfaces for a reservoir state in the silicon valence band. One can estimate the activation barrier for the charge state transition in the classical limit from the intersection of the parabolas. A general feature of the extracted potentials is the difference in oscillator frequency between the neutral and the positive state. This is an important finding, as the expressions that are usually used to fit experimental data are derived assuming linear coupling modes, i.e. $\omega_+ = \omega_0$.

It can be seen that in the primary (dimer) state, the oxygen vacancy has to overcome a large thermal barrier to capture a hole from the silicon valence band, while in the secondary (puckered) state, charging and discharging via the silicon valence level is predicted to require much less thermal excitation. This is in qualitative agreement with what we would expect for an NBTI defect. However, the initial hole capture barrier of ≈2.7 eV appears too large when compared to experimental observations. The hydrogen bridge on the other hand shows a very small transition barrier for the initial hole capture and is even predicted to be more stable in the positive state when the electron Fermi level is near the

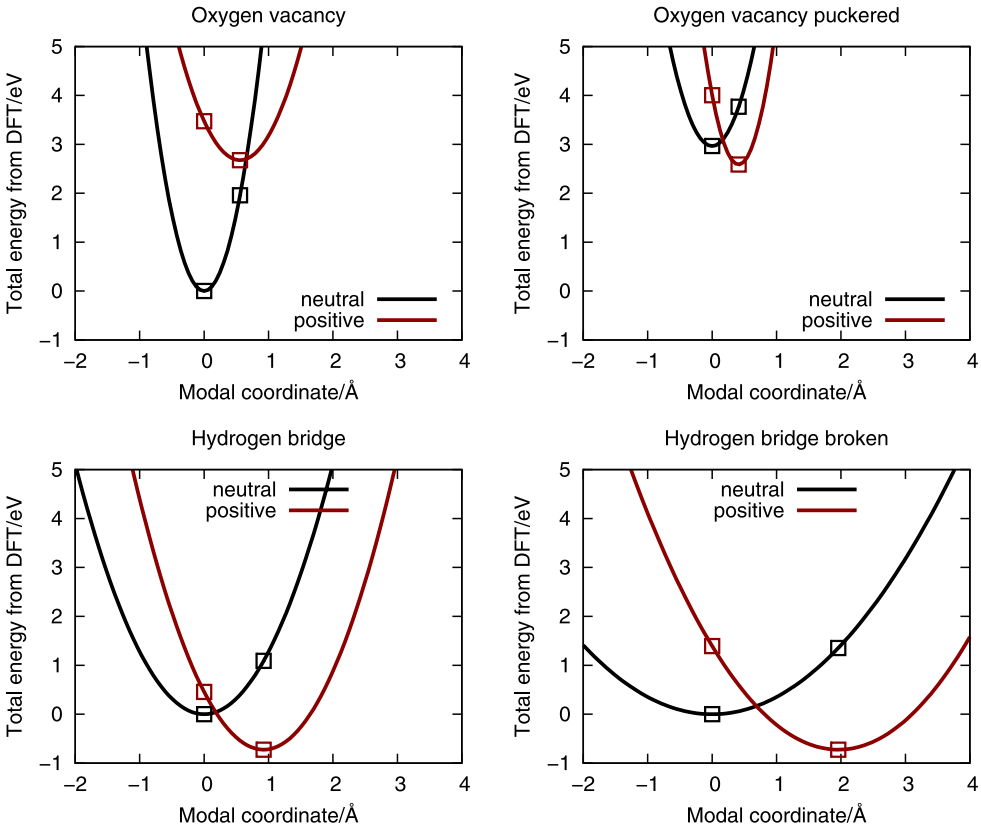

Fig. 4 Potentials for the oxygen vacancy and the hydrogen bridge (reservoir state is the silicon valence band edge). *Symbols* indicate the actual DFT calculations which are used to parametrize the parabolas. All defect configurations except the hydrogen bridge in its primary state show a considerable shift in the oscillator frequency between the two charge states. The activation energy in the classical limit can be estimated from the intersection of the potential energy curves

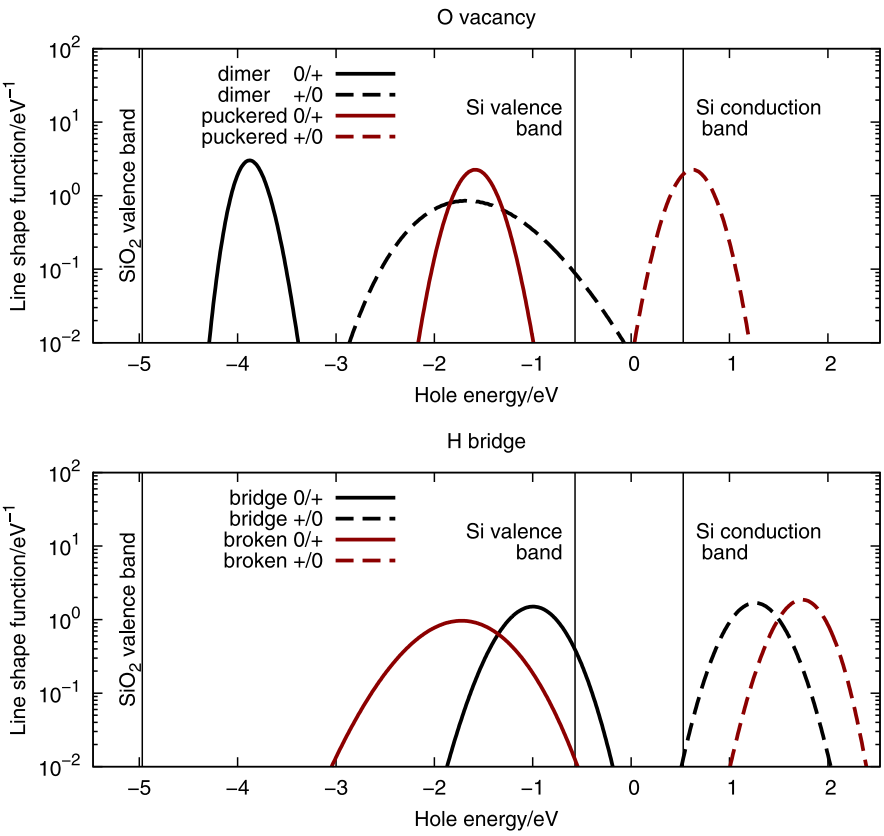

Fig. 5 Line-shape function at 300 K. Life time broadening is simulated by smearing the Dirac peaks of (4) with a normal distribution of standard deviation $k_B T$

silicon valence band, which is also in contradiction to our experimental findings.

The line-shape functions for all transitions are shown in Fig. 5. The plain solution of (4) is a series of weighted Dirac impulses. To account for the non-orthogonality of the selected coupling mode, life-time broadening [3] has been introduced in an empirical manner by smearing of these impulses with a normal distribution of standard deviation $k_B T$.

One can again see a striking difference in the charge capture behavior of the different states of the oxygen vacancy, while this difference is much less pronounced for the hydrogen bridge. Again, the position of the line shape function maximum of the oxygen vacancy for the initial hole capture (dimer $0/+$) is problematic for the explanation of NBTI. The extracted line shape functions will be used in device simulations to assess the behavior of both defects during device operation.

5 Conclusions

The proper description of the behavior of oxide defects involved in NBTI and RT/flicker noise requires the consideration of the thermal motion of the atoms building the defect structure. The physical basis of charge capture and release was discussed and its relation to atomistic modeling and DFT was explained. Charge state transition properties for two defects were calculated in the framework of non radiative multi phonon transition theory. The results can be used to investigate the behavior of the model defects during device operation.

Acknowledgements The authors want to express their gratitude to Alex Shluger, Keith McKenna, Georg Kresse, and Peter Blöchl for valuable discussions. This work has received funding from the EC's FP7 grant agreement n° 216436 (ATHENIS) and from the ENIAC MODERN project n° 820379.

References

1. Shockley, W., Read, W.T.: Phys. Rev. **87**, 835 (1952)
2. Lang, D.V.: J. Appl. Phys. **45**, 3023 (1974)
3. Henry, C.H., Lang, D.V.: Phys. Rev. B **15**(15), 989 (1977)
4. Kirton, M., Uren, M.: Appl. Phys. Lett. **48**, 1270 (1986)
5. Palma, A., Godoy, A., Jemènez-Tejada, J.A., Carceller, J.E., Lòpez-Villanueva, J.A.: Phys. Rev. B **56**(15), 9565 (1997)
6. Zanolla, N., Siprak, D., Baumgartner, P., Sangiorgi, E., Fiegna, C.: In: Proc. Workshop on Ultimate Integration of Silicon, Udine, Italy, pp. 137–140 (2008)
7. Grasser, T., Kaczer, B., Goes, W., Aichinger, T., Hehenberger, P., Nelhiebel, M.: In: Proc. Intl. Rel. Phys. Symp., pp. 33–44 (2009)
8. Wagner, P., Aichinger, T., Grasser, T., Nelhiebel, M., Vandamme, L.: In: Proc. Int. Conf. on Noise and Fluctuations (2009)
9. Kaczer, B., Grasser, T., Martin-Martinez, J., Simoen, E., Aoulaiche, M., Roussel, P., Groeseneken, G.: In: Proc. Intl. Rel. Phys. Symp. (2009)
10. Kaczer, B., Grasser, T., Roussel, P., Franco, J., Degraeve, R., Ragnarsson, L., Simoen, E., Groeseneken, G., Reisinger, H.: In: Proc. Intl. Rel. Phys. Symp., pp. 26–32 (2010)
11. Grasser, T., Reisinger, H., Wagner, P.J., Kaczer, B.: In: Proc. Intl. Rel. Phys. Symp., pp. 16–25 (2010)
12. Blöchl, P.E.: Phys. Rev. B **62**(10), 6158 (2000)
13. Fowler, W.B., Rudra, J.K., Zvanut, M.E., Feigl, F.J.: Phys. Rev. B **41**(12), 8313 (1990)
14. Nicklaw, C.J., Lu, Z.Y., Fleetwood, D., Schrimpf, R., Pantelides, S.: IEEE Trans. Nucl. Sci. **49**, 2667 (2002)
15. Fleetwood, D., Xiong, H., Lu, Z.Y., Nicklaw, C., Felix, J., Schrimpf, R., Pantelides, S.: IEEE Trans. Nucl. Sci. **49**(6), 2674 (2002)
16. Blöchl, P.E., Stathis, J.H.: Phys. Rev. Lett. **83**(2), 372 (1999)
17. Rudra, J.K., Fowler, W.B.: Phys. Rev. B **35**(15), 8223 (1987)
18. Mysovsky, A.S., Sushko, P.V., Mukhopadhyay, S., Edwards, A.H., Shluger, A.L.: Phys. Rev. B **69**(8), 085202 (2004)
19. Kresse, G., Furthmüeller, J.: Phys. Rev. B **54**(11), 11169 (1996)
20. Kresse, G., Joubert, D.: Phys. Rev. B **59**, 1758 (1999)
21. Schanovsky, F., Goes, W., Grasser, T.: J. Vac. Sci. Technol. (2011, submitted)
22. Makram-Ebeid, S., Lannoo, M.: Phys. Rev. B **25**(10), 6406 (1982)
23. Huang, K., Rhys, A.: Proc. R. Soc. A **204**, 406 (1950)
24. Zapol, B.: Chem. Phys. Lett. **93**(6), 549 (1982)
25. Ansbacher, F.: Z. Naturforsch. **14a**, 889 (1959)